Available online at www.sciencedirect.com

ScienceDirect

Advances in Space Research 54 (2014) 1563–1570

ADVANCES IN SPACE RESEARCH (a COSPAR publication)

www.elsevier.com/locate/asr

A VLBI baseline post-adjustment approach for station velocity estimation in Eurasian continent

Zhibin Zhang [a,b,*], Xiang Liu [a]

[a] Xinjiang Astronomical Observatory, CAS, 830011 Urumqi, China
[b] University of Chinese Academy of Sciences, CAS, 100049 Beijing, China

Received 17 December 2013; received in revised form 18 June 2014; accepted 20 June 2014
Available online 28 June 2014

Abstract

Baseline lengths and their time-derivatives among 58 geodetic VLBI stations were fitted by using 4439 observing sessions from the International VLBI Service for Geodesy and Astrometry (IVS). First, the velocities of eight stations in Eurasian continent were set as unknown quantities. Then, two standard global solutions from 3523 IVS sessions and 1110 sessions from database code XA, respectively, were applied prior to all-station coordinates and the non-estimated station velocities. Finally, from the relations among the coordinates, velocities, baseline length and its time-derivative, two types of baseline post-adjustment (BPA) were used to estimate the velocities of the eight stations. We discuss the data processing details, including the effect of different prior values for the stations and the optimal solution.

The results suggest that the precision of the station velocities based on the proposed approach is comparable to that of the global solution of the XA sessions. The baseline structure and the prior values of the stations affect the velocity estimates. Compared to the standard method of velocity estimation, there are no external constrains and conditions used in the proposed method.

Keywords: VLBI; IVS; Baseline post-adjustment; Station velocity

Geodetic Very Long Baseline Interferometry (VLBI) is an effective method for building terrestrial reference frames (TRFs) and studying crustal movements of the Earth. In standard large-scale geodetic data processing for estimating the station velocity, No-net-transform and No-net-rotation (NNT/NNR) conditions are typically used. A set of stations is defined as a datum, and the coordinates and velocities are bound to a TRF to overcome the rank deficiency of the normal matrix, which is caused by the lack of origin positioning and direction orientation in the stations, when we stack the normal matrices after the single session solution, e.g. ITRF (Altamimi et al., 2011) and VTRF (Böckmann et al., 2010). The neglected loading corrections are absorbed by the NNT/NNR conditions (Schuh and Böhm, 2012) in such a restricted parameter adjustment. However, these theoretical assumptions could influence the estimated station coordinates, as reported in Kutterer (2004) and Heinkelmann et al. (2006, 2007). Moreover, it is time consuming to perform the datum test.

As a product of geodetic VLBI, the baseline length is most precisely determined from VLBI data, e.g. Ma et al. (1994). Baseline models are less prone to common systematic effects and consequently simpler than large-scale solutions (Iz and Archinal, 2000). However, baselines find limited use as estimators of the precision of observations, e.g. Titov (2009), or indicators of geodynamic processes, e.g. Herring et al. (1986), Kondo et al. (1998) and Iz (2006). Clearly, it is necessary to develop velocity models to avoid the above-mentioned problems. Moreover, the advantages of the baselines need to be considered.

* Corresponding author at: Xinjiang Astronomical Observatory, CAS, 830011 Urumqi, China.
E-mail address: zhangzhibin@xao.ac.cn (Z. Zhang).

http://dx.doi.org/10.1016/j.asr.2014.06.032
0273-1177/

We used a simple geometry that links the baseline information with the positions and velocities of the stations. Giunchi et al. (1997) calculated the theoretical baseline length time-derivative via the geometry by considering the horizontal velocity on a flat Earth and examined the potential influence of the lateral variations in viscosity upon the observed length component of European VLBI baselines. Yang et al. (2001) picked out eight intra- and intercontinental baselines (precision is ±2 mm/yr) and obtained the velocity of the VLBI station Seshan in Shanghai by considering a geometry similar to that given by Giunchi et al. (1997). However, there are deficiencies in their work, such as inconsistent TRF for the baselines and velocities as well as the bad distribution of the surrounding common observing stations.

In this study, we named the method for estimating the station velocity based on geometry as baseline post-adjustment (BPA). Velocities of eight stations located in the Eurasian continent are the samples. The benefits and limitations of the method are discussed. The proposed BPA method is presented in Section 1. The results and the error analysis are discussed in Section 2, and concluding remarks are summarized in Section 3.

1. The BPA approach

1.1. Equations

We propose Eq. (1) to estimate the site velocities of VLBI stations by using weighted-least-squares (WLS) as follows:

$$\begin{aligned} B_{ij}\dot{B}_{ij} &= (\boldsymbol{r_j} - \boldsymbol{r_i}) \cdot (\dot{\boldsymbol{r}}_j - \dot{\boldsymbol{r}}_i), \\ p_{ij} &= 1/(B_{ij}^2\sigma_{\dot{B}_{ij}}^2 + \dot{B}_{ij}^2\sigma_{B_{ij}}^2), \end{aligned} \tag{1}$$

where B_{ij} and $\dot{B}_{ij}$ are the baseline length and its time-derivative between station i and j, respectively, and $\sigma_{B_{ij}}$ and $\sigma_{\dot{B}_{ij}}$ are the corresponding uncertainties. $\boldsymbol{r_i}$ and $\boldsymbol{r_j}$ are the initial values of the three-dimensional geocentric position vectors for two stations at both ends of the baseline. $\dot{\boldsymbol{r}}_i$ and $\dot{\boldsymbol{r}}_j$ are the three-dimensional geocentric velocity vectors of the two stations, respectively, and p_{ij} is the weight deduced from the baseline length and its time-derivative.

In Eq. (1), $\dot{\boldsymbol{r}}_i$ and $\dot{\boldsymbol{r}}_j$ are treated as unknown. They were sequentially estimated by fixing each one of them (type I: individual estimation) and solved all at once (type II: combined estimation). See the appendix for details.

Moreover, as shown by the weight p_{ij} from the law of error propagation, the uncertainties of the estimated velocities are determined only by the errors of the baseline lengths and their time-derivatives.

1.2. Steps for processing with BPA

The velocities of the eight stations in Eurasian continent are set as unknown quantities at first, see Fig. 1. Then, two kinds of standard global solutions are applied prior to all station coordinates and the non-estimated station velocities. Finally, with Eq. (1), baseline post-adjustment is used to estimate the velocities of the eight stations.

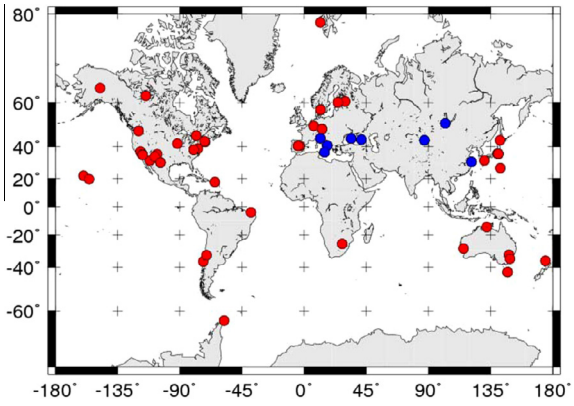

Fig. 1. All 58 stations (dots) including the eight stations (blue dots) with unknown velocities. (For interpretation of the references to color in this figure legend, the reader is referred to the web version of this article.)

Fig. 2 shows the four models: single solution, global solution, baseline fitting, and the BPA. The accuracy and precision of each model can be evaluated by its corresponding χ^2 and WRMS[1] after fitting, respectively.

Initially, 4439 International VLBI Service (IVS) (Schuh and Behrend, 2012) sessions, which cover more than 8 h of observations and 33 years (1980–2012), are solved using the Vienna VLBI Software (VieVS) (Böhm et al., 2009). The baseline information including baseline length, its time-derivative and corresponding errors are extracted from the single solution. Considering the baselines linked to the estimated stations, we increased the number of baselines that satisfies the following baseline exclusion criteria:

- Offsets of baseline points that are five times greater than the mean deviation (formal error) are considered as outliers and are excluded after removing their long-term variation effects.
- A baseline is excluded when the number of baseline observations for a single baseline is less than five.

Baseline information including the baseline length at epoch J2000.0 and its time-derivative as well as their corresponding uncertainties were acquired by WLS fitting. In addition, single solutions with χ^2 less than two were used in the global solutions. Two global solutions give the known values for the BPA. The first global solution is

[1] In this study, χ^2 is defined as $\chi^2 = \left(\sum_{j=1}^{n}\delta_j^2/\sigma_j^2\right)/f$, which can be used to scale the variances of estimates when χ^2 is greater than unity (Herring et al., 1986). Here n is the number of observations for the specific model, δ is the residual from the model fit by WLS, σ is the standard deviation of the observation and f is the number of degrees of freedom. The weighted root-mean-square (WRMS) is defined as $\mathrm{WRMS} = \left[\left(\sum_{j=1}^{n}\delta_j^2/\sigma_j^2\right)/\left(\sum_{j=1}^{n}1/\sigma_j^2\right)\right]^{1/2}$.

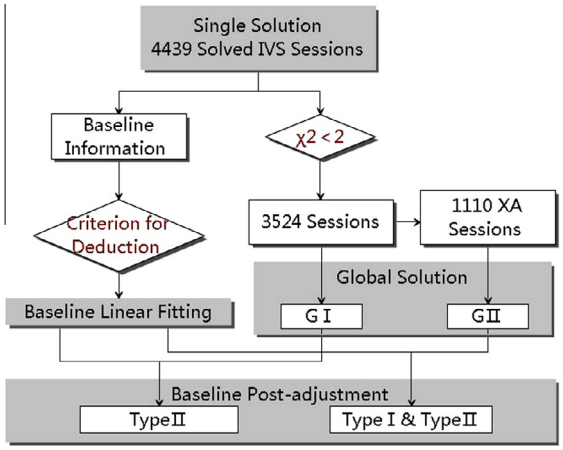

Fig. 2. Flowchart for the two types of BPA solution (blocks in gray denote the applied model).

based on 3524 IVS sessions, which meet the χ^2 requirement and is denoted as G I. The second global solution is based on 1110 sessions with database code (DBC) XA and is denoted as G II. Many papers, e.g. Titov (2002) and Malkin (2009, 2013) indicate that the precision and accuracy of the Earth Orientation Parameters (EOPs) are dependent on factors related to the number of stations, network geometry, and registration mode. Meanwhile, the EOPs provide a link between the celestial reference frame and the TRF. Hence, the above factors which can be distinguished by different DBC types to a certain extent also affect the solution of the position and velocity of stations, e.g. Titov and Tregoning (2005). Because the XA sessions are of the longest span and widest distribution of stations among all DBC types of sessions in general, and the solution (G I) after consolidation of different VLBI networks is probably unsuitable for BPA, 1110 XA sessions were solved as the second global solution (G II) and compared with G I.

Finally, two BPA type II solutions (combined estimations) were estimated by applying the G I and G II as prior values, respectively, and compared with the BPA type I solution (individual estimation), which was estimated by applying G I as a prior value.

2. Results and discussion

To cope with the possible TRF rotation caused by the integration of multiple technologies, VTRF (Böckmann et al., 2010) is taken as the priori terrestrial reference frame. We found that for the UT1 estimate after the single solution based on the XA sessions, the VTRF standard deviation of the IERS C04 series is about 0.5 μs in contrast to 3.8 μs of ITRF2008 (Altamimi et al., 2011), and this difference could give rise to the possible rotation of TRF.

All estimates of each global solution G I or G II, which is based on different number of sessions, are carefully examined to minimize the correlation among them.

As shown in Table 1, the precision of the velocity extracted from G I is obviously higher than that from G II because of the larger amount of observation sessions in G I. However, the χ^2 of the BPA type II solutions can reach up to 38.4 with G I as a prior value, whereas it is only 3.6 with G II as a prior value. Thus, the BPA solution of G I is not considered in this study. This shows that the known values for the G II stations are better suited to the proposed BPA model than the values for G I. The XA sessions include the majority of the observations for most of the stations. Therefore, the baseline information is dominated by the XA sessions. Moreover, sessions with other database codes could generate different results for different observation networks. The following discussion is mainly based on the solution with G II as a prior value.

Two types of BPA solution listed in Table 1 are solved based on the G II as a prior value. The uncertainties of G II and the two corresponding BPA solutions are comparable. Moreover, the BPA type II solution is more stable than type I because the χ^2 of type II is very close to the mean of type I.

2.1. Baseline uncertainty

The baseline precision depends on its length. Because of the shorter the baseline, there is broader common sky containing more common sources that are scanned by the two stations of baseline. Hence, more low elevation observations can be well sampled to reduce the impact of tropospheric asymmetry. In addition, the antenna slew rate at the source is also critical to the baseline precision (Titov, 2009). To evaluate precision, the number of times VLBI participates also contributes to the baseline precision. Stations set up for astrometry and space exploration (e.g. Urumqi) devote limited time to geodetic observations; thus, the velocity uncertainties for these stations will be high. In the VLBI observations, systematic instrument errors and unaccounted atmospheric and earthquake errors add to the uncertainties.

Theoretically, there are 428 baselines linked to the eight stations among 58 stations (Fig. 1). However, restricted by the arrangements in observational schedules and the baseline exclusion criteria, only 224 baselines can be used for the type II BPA. The average uncertainties of the baseline length at J2000.0 and of the length time-derivative are ±29.2 mm and ±3.5 mm/yr, respectively.

2.2. Optimal BPA solution

When we increase the threshold of χ^2, denoted as T_{χ^2}, for a priori baseline refinement, more baselines will be included in the BPA. Consequently, the baseline distribution is more stable and the precision of the BPA solution increases. Moreover, baselines that cannot be well modeled will lower the precision of the BPA solution, implying that there must be an optimal T_{χ^2} for excluding bad baselines.

Table 1
The topocentric velocity solutions from the global solutions and the two different BPA types based on G II for the eight stations with respect to the geocenter.

Station name		G I (mm/yr)	G II (mm/yr)	Type I (mm/yr)	Type I χ^2	Type II χ^2=3.6
Medicina	E	21.1 ± 0.0	20.8 ± 0.3	20.6 ± 0.2	3.7	20.7 ± 0.1
	N	16.2 ± 0.0	14.4 ± 0.2	14.5 ± 0.2		14.5 ± 0.2
	U	−1.0 ± 0.1	0.5 ± 0.3	1.0 ± 0.2		0.8 ± 0.2
Matera	E	22.1 ± 0.0	21.6 ± 0.3	21.6 ± 0.2	8.1	21.7 ± 0.1
	N	17.6 ± 0.0	15.8 ± 0.2	15.8 ± 0.2		15.8 ± 0.2
	U	0.9 ± 0.1	2.5 ± 0.3	2.5 ± 0.2		2.6 ± 0.2
Noto	E	20.0 ± 0.1	19.4 ± 0.3	19.0 ± 0.6	7.3	19.0 ± 0.4
	N	18.3 ± 0.0	16.7 ± 0.2	16.6 ± 1.0		16.8 ± 0.7
	U	0.5 ± 0.2	2.2 ± 0.4	2.9 ± 1.1		3.2 ± 0.8
Crimea	E	23.0 ± 0.1	21.6 ± 0.4	20.6 ± 0.7	2.2	21.8 ± 0.6
	N	11.0 ± 0.1	9.1 ± 0.3	7.8 ± 1.0		8.7 ± 1.1
	U	1.5 ± 0.3	2.8 ± 0.5	−0.6 ± 1.0		0.8 ± 1.1
Zelenchukskaya	E	23.4 ± 0.9	18.0 ± 1.2	21.0 ± 0.4	0.8	21.4 ± 0.5
	N	12.3 ± 1.0	12.4 ± 1.2	5.8 ± 0.6		7.4 ± 0.8
	U	5.4 ± 4.0	6.9 ± 4.8	4.1 ± 0.6		4.7 ± 0.8
Urumqi	E	21.9 ± 0.1	25.5 ± 0.6	23.1 ± 1.4	3.8	24.9 ± 0.8
	N	3.3 ± 0.1	4.2 ± 0.5	3.6 ± 1.7		5.0 ± 1.7
	U	6.4 ± 0.3	3.9 ± 0.5	4.3 ± 1.6		4.6 ± 1.6
Badary	E	19.7 ± 0.2	19.6 ± 0.6	21.4 ± 1.1	1.3	19.8 ± 0.8
	N	−9.0 ± 0.2	−8.3 ± 0.6	−7.5 ± 1.7		−8.7 ± 1.4
	U	7.4 ± 0.5	2.1 ± 1.0	2.4 ± 1.9		3.7 ± 1.6
Seshan	E	29.1 ± 0.0	23.6 ± 0.6	21.3 ± 0.6	2.0	21.7 ± 0.5
	N	−12.8 ± 0.1	−14.1 ± 0.7	−14.4 ± 1.0		−14.3 ± 0.7
	U	−1.4 ± 0.1	−0.7 ± 0.4	0.0 ± 0.8		−0.4 ± 0.6
Avg. error		± 0.3	±1.3	±1.5	3.6	± 1.3

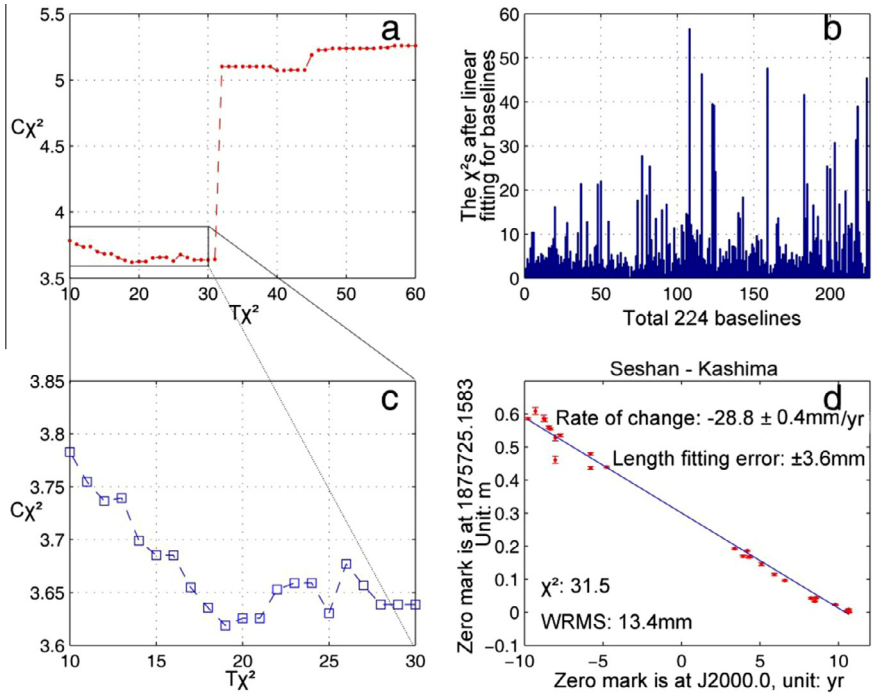

Fig. 3. The threshold test for baseline exclusion and corresponding χ^2. The lowest point is not obvious in (a). The χ^2s of the baselines are shown in (b). The area between 10–30 in (a) is enlarged in (c); consequently, the lowest point (T_{χ^2} at 19) becomes clear and is taken as the optimal threshold. The obvious leap in (a) is caused by the Seshan–Kashima baseline, which is shown in (d). T_{χ^2} less than 10 is not shown because it results in singular matrices.

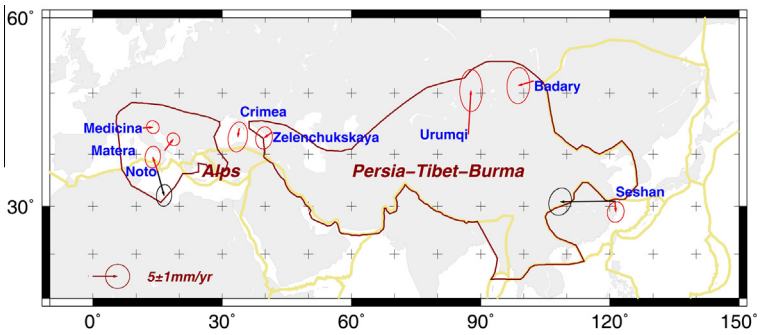

Fig. 4. Horizontal velocity differences (red arrows) at epoch 2000.0 between BPA type II solution and NNR-MORVEL (model errors are generally ±0.5 mm/yr in the east and north directions) when the Eurasia plate is the background field. Black arrows for Noto and Seshan are velocity differences with respect to the velocity fields of their own plates (Nubia and Yangze) defined by NNR-MORVEL, respectively. The areas marked with dark red curves are the Alps and the Persia-Tibet-Burma orogenic belts (Bird, 2003). Yellow curves are deviation for the plate boundaries of tectonic plates deviation (Argus et al., 2011). The ellipses represent 95% confidence level. Except for Crimea, all stations show significant relative motion. (For interpretation of the references to color in this figure legend, the reader is referred to the web version of this article.)

For type II BPA solutions, different T_{χ^2}s and their corresponding χ^2s, denoted as C_{χ^2}, were tested (Fig. 3). First, C_{χ^2} gradually decreases with increasing T_{χ^2} and then C_{χ^2} increases erratically due to the effect of the baselines with larger χ^2s. The lowest point in Fig. 3(a) and (c) is the equilibrium point for baseline distribution stability and excluding bad baselines. Both types of BPA results listed in Table 1 are based on their individual optimal threshold.

2.3. Station site movement

The movement of stations relative to NNR-MORVEL[2] (Argus et al., 2011), which is a set of angular velocities of the 25 MORVEL plates relative to the NNR reference frame, are shown in Fig. 4. Combined with Table 1, we can infer the following.

1. The differences in the number of stations in northern and southern hemispheres cause the major axis of the error ellipses to have a north–south direction. The up components pointing to the respective zeniths of the eight stations are significantly greater than the east-pointing components because the up components are determined by the intersection of the one side baselines.
2. Regarding to the velocity uncertainties of the stations, the four stations, Medicina, Matera, Crimea (also known as Simeiz) and Seshan are in good agreement with the G II and both types of corresponding BPA solutions.
3. For Zelenchukskaya, the velocity uncertainty for G II was piecewisely estimated and the result was lower for the BPA because the global solutions in Table 1 are obtained from short observation sessions. In contrast to its long-spanning solution (22.9 ± 0.4E, 5.3 ± 0.3 N, 1.5 ± 0.6U, unit: mm/yr), there is good consistency in the velocity in the east and north directions.
4. The relative movements of the stations near the Eurasian boundary need to be further investigated, e.g. Seshan is the fastest moving station among the eight stations when the Yangze plate is chosen as its background, whereas the Eurasian plate seems more reasonable when considering its velocity magnitude. The same arguments hold for Noto.
5. The baseline lengths, the number of baselines, and the distribution of baselines mainly control the uncertainties in the velocity of stations. The station velocity with relatively large error is due to the sparse baseline structure and the lack of short baselines clusters around such stations (Fig. 5), e.g. Urumqi and Badary. Avouac et al.

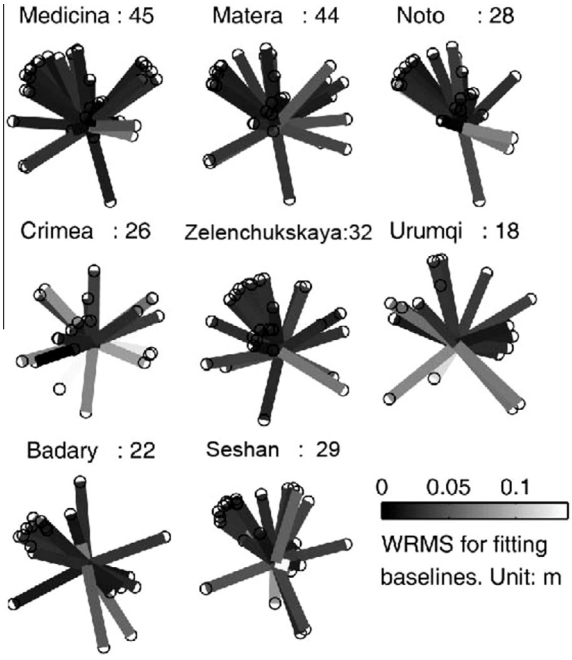

Fig. 5. Baseline structures viewed from their individual local zenith (the legend on top of each diagram gives the station name and the number of connected baselines) and their fitted WRMSs for baselines.

[2] http://geoscience.wisc.edu/~chuck/MORVEL/index.html.

(1993) suggested that the rate of shortening across the Tien Shan subplate is at least 6 ± 3 mm/yr at longitude ~ 85.5°E, while the horizontal velocity of Urumqi (~ 87.2°E) after BPA is 8.9 ± 2.0 mm/yr with respect to the Eurasian plate. There is a good agreement between them. The velocity uncertainty in Crimea is not well constrained probably because of the relatively limited time in the geodetic VLBI observations.

3. Conclusions

The proposed BPA method is based on linear intersection, which is rather intuitive and does not require external constrains and other conditions typically used in conventional methods. Furthermore, the non-estimated stations are a datum in the normal matrix for estimating the velocity. The main conclusions of this study can be summarized as follows:

1. Currently, the precisions of station velocities, which are calculated from two types of the baseline post-adjustment solutions and defined by the average uncertainties (±1.5 mm/yr and ±1.3 mm/yr, respectively) of the velocities of the stations, are comparable to the uncertainty (±1.3 mm/yr) of the global solution, which is based on XA sessions.
2. The baselines connected to the estimated stations, the prior values of station positions, and velocities all affect the uncertainty of the BPA results. The precision of the station velocity will improve when more high-precision baselines and greater baseline coverage are added to the BPA model.
3. For both types of BPA, we obtain more stable errors by solving all estimated stations once (type II) than solving them one-by-one (type I). The choice of the threshold for excluding bad baselines and obtaining an optimal solution can also be taken as reference.
4. The velocities of the eight stations confirms the division of the orogenic belts in Eurasia; nonetheless, several boundary stations (Noto and Seshan) need to be further studied.

Acknowledgments

We greatly acknowledge the referee for his valuable suggestions and questions. IVS is thanked for the session coordination. Several plots were made with the General Mapping Tool (GMT) software (Wessel and Smith 1998), available at http://gmt.soest.hawaii.edu under the GNU General Public License. This work was supported in part by the National Natural Science Foundation of China (Grant No. 11273050).

Appendix

Two types of BPA equations corresponding to Eq. (1) are expanded into Eqs. (A.1) and (A.2), respectively, in which, the elements with superscript '0' in the matrices or vectors denote the velocities or positions of non-estimated stations. For estimated stations, their coordinates are known but their velocities need to be determined. Each element, $\boldsymbol{r}$ or $\dot{\boldsymbol{r}}$, contains three geocentric coordinate components. $\boldsymbol{x}$ denotes the estimated vector. A is design matrix and $\boldsymbol{l}$ is the right-hand-side vector.

For BPA type I, there is only one station velocity to be estimated. N_e is the number of the baselines linked to the estimated station e. B_{ei} and $\dot{B}_{ei}$, with $i = 1, 2, \ldots, N_e$, which are made up of station e and the other stations, denote the baseline length and its time-derivative, respectively. $(\cdot)_{x,y\ or\ z}$ denotes the corresponding component of the vector.

For BPA type II, all u station velocities are estimated together. The corresponding components have not been expanded in Eq. (A.2). n_i, with $i = 1, 2, \ldots, u$, denotes the number of baselines, which are made up of station i and the linked non-estimated stations. N_B is the total number of baselines joint in the type II solution. The content above the separator line in A and $\boldsymbol{l}$ reflects the relations among estimates while the content below the separator line reflects the relations among the estimated stations and the other stations. The blank area in A are zero elements.

$$\text{Type I}: \underbrace{\begin{pmatrix} (\boldsymbol{r}_e - \boldsymbol{r}_1^0)_x & (\boldsymbol{r}_e - \boldsymbol{r}_1^0)_y & (\boldsymbol{r}_e - \boldsymbol{r}_1^0)_z \\ (\boldsymbol{r}_e - \boldsymbol{r}_2^0)_x & (\boldsymbol{r}_e - \boldsymbol{r}_2^0)_y & (\boldsymbol{r}_e - \boldsymbol{r}_2^0)_z \\ \vdots & & \\ (\boldsymbol{r}_e - \boldsymbol{r}_{N_e}^0)_x & (\boldsymbol{r}_e - \boldsymbol{r}_{N_e}^0)_y & (\boldsymbol{r}_e - \boldsymbol{r}_{N_e}^0)_z \end{pmatrix}}_{\begin{array}{c}\| \\ A \\ N_e \times 3\end{array}} \underbrace{\begin{pmatrix} (\dot{\boldsymbol{r}}_e)_x \\ (\dot{\boldsymbol{r}}_e)_y \\ (\dot{\boldsymbol{r}}_e)_z \end{pmatrix}}_{\begin{array}{c}\| \\ \boldsymbol{x} \\ 3 \times 1\end{array}} = \underbrace{\begin{pmatrix} B_{e1}\dot{B}_{e1} + (\boldsymbol{r}_e - \boldsymbol{r}_1^0) \cdot \dot{\boldsymbol{r}}_1^0 \\ B_{e2}\dot{B}_{e2} + (\boldsymbol{r}_e - \boldsymbol{r}_2^0) \cdot \dot{\boldsymbol{r}}_2^0 \\ \vdots \\ B_{eN_e}\dot{B}_{eN_e} + (\boldsymbol{r}_e - \boldsymbol{r}_{N_e}^0) \cdot \dot{\boldsymbol{r}}_{N_e}^0 \end{pmatrix}}_{\begin{array}{c}\| \\ \boldsymbol{l} \\ N_e \times 1\end{array}}. \tag{A.1}$$

$$\text{Type II}: \underbrace{\left[\begin{array}{cccccc} \boldsymbol{r_1}-\boldsymbol{r_2} & -(\boldsymbol{r_1}-\boldsymbol{r_2}) & & & & \\ \boldsymbol{r_1}-\boldsymbol{r_3} & & -(\boldsymbol{r_1}-\boldsymbol{r_3}) & & & \\ \vdots & & & \ddots & & \\ \boldsymbol{r_1}-\boldsymbol{r_u} & & & & & -(\boldsymbol{r_1}-\boldsymbol{r_u}) \\ & \boldsymbol{r_2}-\boldsymbol{r_3} & -(\boldsymbol{r_2}-\boldsymbol{r_3}) & & & \\ & \vdots & & \ddots & & \\ & \boldsymbol{r_2}-\boldsymbol{r_u} & & & & -(\boldsymbol{r_2}-\boldsymbol{r_u}) \\ & & & \ddots & & \vdots \\ & & & & \boldsymbol{r_{u-1}}-\boldsymbol{r_u} & -(\boldsymbol{r_{u-1}}-\boldsymbol{r_u}) \\ \hline \boldsymbol{r_1}-\boldsymbol{r}^0_{u+1} & & & & & \\ \vdots & & & & & \\ \boldsymbol{r_1}-\boldsymbol{r}^0_{n_1} & & & & & \\ & \boldsymbol{r_2}-\boldsymbol{r}^0_{u+1} & & & & \\ & \vdots & & & & \\ & \boldsymbol{r_2}-\boldsymbol{r}^0_{n_2} & & & & \\ & & & \ddots & & \\ & & & & \boldsymbol{r_u}-\boldsymbol{r}^0_{u+1} & \\ & & & & \vdots & \\ & & & & \boldsymbol{r_u}-\boldsymbol{r}^0_{n_u} & \end{array}\right]}_{\substack{A \\ N_B\times 3u}} \underbrace{\left[\begin{array}{c} \dot{\boldsymbol{r}}_1 \\ \dot{\boldsymbol{r}}_2 \\ \vdots \\ \dot{\boldsymbol{r}}_u \end{array}\right]}_{\substack{\boldsymbol{x} \\ 3u\times 1}} = \underbrace{\left[\begin{array}{c} B_{12}\dot{B}_{12} \\ B_{13}\dot{B}_{13} \\ \vdots \\ B_{1u}\dot{B}_{1u} \\ B_{23}\dot{B}_{23} \\ \vdots \\ B_{2u}\dot{B}_{2u} \\ \vdots \\ B_{u-1\,u}\dot{B}_{u-1\,u} \\ \hline B_{1\,u+1}\dot{B}_{1\,u+1}+(\boldsymbol{r_1}-\boldsymbol{r}^0_{u+1})\cdot\dot{\boldsymbol{r}}^0_{u+1} \\ \vdots \\ B_{1\,n_1}\dot{B}_{1\,n_1}+(\boldsymbol{r_1}-\boldsymbol{r}^0_{n_1})\cdot\dot{\boldsymbol{r}}^0_{n_1} \\ B_{2\,u+1}\dot{B}_{2\,u+1}+(\boldsymbol{r_2}-\boldsymbol{r}^0_{u+1})\cdot\dot{\boldsymbol{r}}^0_{u+1} \\ \vdots \\ B_{2\,n_2}\dot{B}_{2\,n_2}+(\boldsymbol{r_2}-\boldsymbol{r}^0_{n_2})\cdot\dot{\boldsymbol{r}}^0_{n_2} \\ \vdots \\ B_{u\,u+1}\dot{B}_{u\,u+1}+(\boldsymbol{r_u}-\boldsymbol{r}^0_{u+1})\cdot\dot{\boldsymbol{r}}^0_{u+1} \\ \vdots \\ B_{u\,n_u}\dot{B}_{u\,n_u}+(\boldsymbol{r_u}-\boldsymbol{r}^0_{n_u})\cdot\dot{\boldsymbol{r}}^0_{n_u} \end{array}\right]}_{\substack{\boldsymbol{l} \\ N_B\times 1}} \tag{A.2}$$

Then, the valuation vector $\hat{\boldsymbol{x}}$ for the estimated vector $\boldsymbol{x}$ of two BPA types is as follows:

$$\hat{\boldsymbol{x}} = (A^T P A)^{-1}(A^T P \boldsymbol{l}), \tag{A.3}$$

where P is the weight matrix in Eq. (A.4).

$$P = \begin{cases} \begin{pmatrix} \frac{1}{B^2_{e1}\sigma^2_{\dot{B}_{e1}}+\dot{B}^2_{e1}\sigma^2_{B_{e1}}} & & & \\ & \frac{1}{B^2_{e2}\sigma^2_{\dot{B}_{e2}}+\dot{B}^2_{e2}\sigma^2_{B_{e2}}} & & \\ & & \ddots & \\ & & & \frac{1}{B^2_{eN_e}\sigma^2_{\dot{B}_{eN_e}}+\dot{B}^2_{eN_e}\sigma^2_{B_{eN_e}}} \end{pmatrix}_{N_e\times N_e}, & \text{for type I} \\ \begin{pmatrix} \frac{1}{B^2_{12}\sigma^2_{\dot{B}_{12}}+\dot{B}^2_{12}\sigma^2_{B_{12}}} & & & \\ & \frac{1}{B^2_{13}\sigma^2_{\dot{B}_{13}}+\dot{B}^2_{13}\sigma^2_{B_{13}}} & & \\ & & \ddots & \\ & & & \frac{1}{B^2_{un_u}\sigma^2_{\dot{B}_{un_u}}+\dot{B}^2_{un_u}\sigma^2_{B_{un_u}}} \end{pmatrix}_{N_B\times N_B}, & \text{for type II} \end{cases} . \tag{A.4}$$

The corresponding error σ_x for the valuation vector $\hat{\boldsymbol{x}}$ is as follows:

$$\begin{aligned} \sigma_x^2 &= \sigma_0^2(A^T P A)^{-1}, \\ \sigma_0^2 &= (A\hat{\boldsymbol{x}}-\boldsymbol{l})^T P(A\hat{\boldsymbol{x}}-\boldsymbol{l})/f, \\ f &= \begin{cases} N_e-3, & \text{for type I} \\ N_B-3u, & \text{for type II} \end{cases}, \end{aligned} \tag{A.5}$$

where $(\cdot)^T$ and $(\cdot)^{-1}$ represent the matrix transposition and inversion, respectively.

References

Altamimi, Z., Collilieux, X., Méivier, L., 2011. ITRF2008: an improved solution of the international terrestrial reference frame. J. Geod. 85 (8), 457–473. http://dx.doi.org/10.1007/s00190-011-0444-4.

Argus, F., Gordon, G., DeMets, C., 2011. Geologically current motion of 56 plates relative to the no-net-rotation reference frame. Geochem. Geophys. Geosyst. 12 (11), 1525–2027. http://dx.doi.org/10.1029/2011GC003751.

Avouac, P., Tapponnier, P., Bai, M., You, H., Wang, G., 1993. Active thrusting and folding along the northern Tien Shan and Late Cenozoic rotation of the Tarim relative to Dzungaria and Kazakhstan. J. Geophys. Res.: Solid Earth 98 (B4), 6755–6804. http://dx.doi.org/10.1029/92jb01963.

Bird, P., 2003. An updated digital model of plate boundaries. Geochem. Geophys. Geosyst. 4 (3), 1027. http://dx.doi.org/10.1029/2001GC000252.

Böckmann, S., Artz, T., Nothnagel, A., 2010. VLBI terrestrial reference frame contributions to ITRF2008. J. Geod. 84 (3), 201–219. http://dx.doi.org/10.1007/s00190-009-0357-7.

Böhm, J., Böhm, S., Nilsson, T., Pany, A., Plank, L., Spicakova, H., Teke, K., Schuh, H., 2009. The new Vienna VLBI Software VieVS. In: Kenyon, S., Pacino, M.C., Marti, U. (Eds.), Proceedings of IAG Scientific Assembly 2009, International Association of Geodesy Symposia Series, vol. 136, pp. 1007–1011. http://dx.doi.org/10.1007/978-3-642-20338-1_126.

Giunchi, C., Spada, G., Sabadini, R., 1997. Lateral viscosity variations and post-glacial rebound: eeffects on present-day VLBI baseline deformations. Geophys. Res. Lett. 24 (1), 13–16. http://dx.doi.org/10.1029/96GL03773.

Heinkelmann, R., Tanir, E., Böhm, J., Schuh, H., 2006. The influence of geodetic datum definition on the VLBI reference frames. Geodetic week, October 10–12, Munich, Germany. <http://www.hg.tuwien.ac.at/Bibl_Docs/Posters/2006/2006_GW2006_heinkelmann_po.pdf>.

Heinkelmann, R., Böhm, J., Schuh, H., 2007. Effects of geodetic datum definition on the celestial and terrestrial reference frames determined by VLBI. In: Proceedings of the 18th European VLBI for Geodesy and Astrometry Working Meeting. Technische Universität Wien, vol. 79, pp. 200–205. <http://www.researchgate.net/publication/237772508>.

Herring, T., Shapiro, I., Clark, T., Ma, C., Ryan, J., Schupler, B., Knight, C., Lundqvist, G., Shaffer, D., Vandenberg, N., Corey, B., Hinteregger, H., Rogers, A., Webber, J., Whitney, A., Elgered, G., Ronnang, B., Davis, J., 1986. Geodesy by radio interferometry: evidence for contemporary plate motion. J. Geophys. Res.: Solid Earth B 8 (91), 8341–8347. http://dx.doi.org/10.1029/JB091iB08p08341.

Iz, B., 2006. Differencing reveals hidden changes in baseline length time-series. J. Geod. 80 (5), 259–269. http://dx.doi.org/10.1007/s00190-006-0066-4.

Iz, B., Archinal, A., 2000. VLBI baseline rates from baseline measurements of collocated antennas using composite models. In: Vandenberg, R.N., Baver, K.D. (Eds.), International VLBI Service for Geodesy and Astrometry 2000 General Meeting Proceedings, NASA/CP-2000-209893, pp. 362–367. <http://ivscc.gsfc.nasa.gov/publications/gm2000/iz/>.

Kondo, T., Kurihara, N., Koyama, Y., Sekido, M., Ichikawa, R., Yoshino, T., Amagai, J., Sebata, K., Furuya, M., Takahashi, Y., 1998. Evaluation of repeatability of baseline lengths in the VLBI network around the Tokyo metropolitan area. Geophys. Res. Lett. 7 (25), 1047–1050. http://dx.doi.org/10.1029/98GL50566.

Kutterer, H., 2004. Reliability measures for geodetic VLBI products. In: Vandenberg, R.N., Baver, K.D. (Eds.), International VLBI Service for Geodesy and Astrometry 2004 General Meeting Proceedings. NASA/CP-2004-212255, pp. 301–305. <http://ivscc.gsfc.nasa.gov/publications/gm2004/kutterer>.

Ma, C., Ryan, J.W., Caprette, D.S., 1994. NASA Space Geodesy Program-GSFC Data Analysis -1993, NASA Tech Memo. 104605.

Malkin, Z., 2009. On comparison of the Earth orientation parameters obtained from different VLBI networks and observing programs. J. Geod. 83 (6), 547–556, <http://arxiv.org/abs/0908.1793>.

Malkin, Z., 2013. Impact of seasonal station motions on VLBI UT1 intensives results. J. Geod. 87 (6), 505–514. http://dx.doi.org/10.1007/s00190-013-0624-5.

Schuh, H., Behrend, D., 2012. VLBI: a fascinating technique for geodesy and astrometry. J. Geodyn. 61, 68–80. http://dx.doi.org/10.1016/j.jog.2012.07.007.

Schuh, H., Böhm, J., 2012. Very long baseline interferometry for geodesy and astrometry. In: Xu, G. (Ed.), Sciences of Geodesy II, Innovations and Future Developments. Springer Verlag, ISBN 978-3-642-27999-7, pp. 339–376. http://dx.doi.org/10.1007/978-3-642-28000-9.

Titov, O., 2002. Analysis of the EOPs from Independent Parallel VLBI Sessions. In: Vistas for Geodesy in the New Millennium (International Association of Geodesy Symposia), vol. 125, pp. 440–444. http://dx.doi.org/10.1007/978-3-642-28000-9.

Titov, O., 2009. A new estimator for VLBI baseline length repeatability. J. Geod. 83 (11), 1041–1049. http://dx.doi.org/10.1007/s00190-009-0322-5.

Titov, O., Tregoning, P., 2005. Effect of post-seismic deformation on earth orientation parameter estimates from VLBI observations: a case study at Gilcreek, Alaska. J. Geod. 79 (4–5), 196–202. http://dx.doi.org/10.1007/s00190-005-0459-9.

Yang, Z., Zhu, W., Cheng, Z., 2001. Determination and discussion of motion of Shanghai VLBI station relative to Eurasia plate. Acta Geodaetica et Cartographica Sinica (in Chinese) 30 (1), 10–15.